ChemComm

COMMUNICATION

View Article Online
View Journal | View Issue

Cite this: *Chem. Commun.*, 2024, **60**, 13538

Received 17th July 2024,
Accepted 7th October 2024

DOI: 10.1039/d4cc03549f

rsc.li/chemcomm

3D-printed photothermal-responsive shape-memory polymer for soft robotic applications†

Kalyan Ghosh * and Sohini Kar-Narayan *

In this work, a photocurable resin is formulated for masked stereolithography 3D printing of shape-memory polymers that results in 4D printed customized tools for soft robotics applications, in which actuation is demonstrated at near ambient temperatures as programmed by photothermal heating.

The use of robots has been growing dramatically in recent years in applications ranging from industrial production management to automotive, healthcare, medical operations, and household appliances.[1–3] Conventional hard robots have hinges, bolts, chains and other components to control their motions.[4] However, this gives rise to limitations in operation when working in close contact with the human body or with soft materials. There are several benefits of using soft robots over hard robots from the point of view of safety, and also the multiple degrees of freedom available to change their orientation.[5–7] In terms of fabrication, 3D printing as a manufacturing method has garnered significant interest for its ability to quickly prototype any product by creating it layer by layer, thereby eliminating the labour-intensive steps involved in conventional manufacturing processes.[8] 3D printing enables the facile fabrication of complex-shaped robotic tools.

3D-printing of shape-memory polymers (SMPs) results in 4D printing whereby the 3D-printed object undergoes a predefined transformation in its shape over time by applying external stimuli such as heat, light, magnetic and electric fields.[9] In the context of 4D printing, "time" is introduced as an additional element in the dimensional structure. 4D printing technology offers significant potential in various technological domains such as construction, biomedical engineering, soft robotics, functional textiles, and electrical devices as it utilizes stimuli-responsive materials that can bend, spiral, fold, and twist.[10–12] There are several 3D printing techniques such as stereolithography (SLA), fused deposition modeling (FDM), ink-jet printing, and selective laser sintering (SLS), that have been often used to print SMPs.[11,13] Of these, the SLA technique is particularly attractive as an effective printing method with the highest possible resolution. In SLA printing, a photocurable resin is polymerized layer-by-layer upon exposure to ultraviolet (UV) light, often called vat photopolymerization.[14,15] In the family of vat photopolymerization techniques, digital light processing (DLP), and projection micro stereolithography (PμSL) have been investigated for the printing of stimuli-responsive polymers.[16–19] More recently, masked SLA (mSLA) has emerged as a potentially efficient printing method because of the associated rapid printing time and high surface resolution.[20] The process involves exposing a photosensitive liquid polymer resin to UV light to cure an entire layer of the object at once, selectively controlling the printing area through a liquid crystal display (LCD).[21] So far, several reports have demonstrated DLP, SLA and PμSL printing of SMPs employing customized resins that were mainly formulated by acrylate and methacrylate derivatives.[17,18,22] The reported methacrylate-based heat-responsive SMPs have been shown to typically undergo shape-transformation around 60–90 °C. The heating of the printed objects is often carried out using a hot water bath.[17,18] However, such a heating method to achieve temperatures above 60 °C is often not convenient in practical soft robotic applications. In the case of light-responsive SMPs, the actuation has been shown to occur either by a photothermal effect, such as plasmonic heating, or by a photochemical effect caused by UV/infra-red (IR) light.[23–25] However, stimulation of soft robotic tools by UV light limits their vast potential application when in contact with living tissue.

In this report, a photocurable resin is formulated for mSLA printing of SMP that provides 4D printing to obtain tools for soft robotic applications. The resin was formulated varying the monomer to crosslinker ratio to secure shape transformation at near ambient temperature. The T_g of the polymer at near ambient temperature ($\approx$18 °C) enables shape transformation using a heat lamp at a temperature $\approx$45 °C. For demonstration, we printed several tools, such as a rod with spiral end, a sheet with honeycomb patterns, a pipe elbow, 4-finger grippers and a 4-legged object as shown in Fig. S1 (ESI†). The one-way reversible physical transformation of the

Department of Materials Science and Metallurgy, University of Cambridge, 27 Charles Babbage Rd, Cambridge CB3 0FS, UK. E-mail: kg533@cam.ac.uk, sk568@cam.ac.uk

† Electronic supplementary information (ESI) available: Experimental section, Fig. S1–S9, eqn (S1)–(S3) and Table S1. See DOI: https://doi.org/10.1039/d4cc03549f

printed tools is exhibited by programming simply switching on the heat lamp for ≈2 min to reach a temp of ≈45 °C. The utilization of photothermal heating for shape transformation eliminates the need for traditional heating methods such as hot water or the use of UV light for photoresponsive shape-memory polymers, and additionally, it eliminates the necessity of a specialized enclosed environment for safety purposes. This near-ambient temperature transformation of 3D-printed SMP tools using a heat lamp facilitates real-life application.

For the mSLA printing, a photocurable resin was prepared by mixing benzyl methacrylate (BMA) as monomer and polyethyleneglycol dimethacrylate (PEGDMA, M_n = 750 g mol^{-1}) as crosslinker and diphenyl (2,4,6-trimethyl benzoyl) phosphine oxide (TPO) as initiator following a modified procedure of photocurable resin preparation by Zhang *et al.*[18] The details about materials, fabrication methods and materials characterization are included in ESI.† An 'Original Prusa SL1S Speed' 3D printer (Prusa Research, Czech Republic) equipped with a 405 nm UV LED array was used for the printing. Four different formulations were prepared varying the monomer to crosslinker mass ratio of 1 : 0.33, 1 : 0.50, 1 : 0.75 and 1 : 1. The initiator amount was kept at 2.5 wt% (w/w) with respect to the total monomer and crosslinker amount. The printed polymers with monomer to crosslinker mass ratios of 1 : 0.33, 1 : 0.5, 1 : 0.75 and 1 : 1 are denoted as $SMP_{0.33}$, $SMP_{0.50}$, $SMP_{0.75}$ and $SMP_{1.0}$, respectively. All the SMPs are post-cured at 40 °C for 20 min. Of all the SMP formulations, the printed parts of $SMP_{0.33}$ were found to have many surface defects (Fig. S2, ESI†).

A schematic diagram of the m-SLA printing is shown in Fig. 1a. The light source is masked by an LCD to selectively print the whole single layer of the model at once. The UV light breaks the initiator into reactive radicals that initiate the photopolymerization process. The layer-by-layer printing process allows localized polymerization by which monomers and crosslinkers connect by covalent bond resulting solid network. The chemical structures of the monomer, crosslinker, initiator and polymer network are shown in Fig. S3 (ESI†).

To print a customized resin, it is essential to identify the exact exposure time for curing. The Prusa SL1S printer comprises a 'resin calibration' feature which allows assessing the quality of a set of printed objects being cured for a varied duration of time. The printing guidelines are available on the Prusa Research website.[26] Herein, 8 objects are printed using $SMP_{0.50}$ resin with a UV exposure time of 11 to 25 s with an increase of 2 s for the subsequent prints, keeping a constant 35 s of exposure time for the first layer (Fig. 2a). It was found that at lower exposure times from 11 to 21 s, the parts were not printed correctly, and had many defects. Comparing the printed parts with the original model, we identified that 23 and 25 s of exposure times provide the best print quality. We selected 23 s of exposure time for printing the SMP tools. Separately, the UV exposure time for the first layer was also varied at 25, 30, 35 and 40 s keeping 23 s exposure time for the rest of the layers to affix the printed object with the build platform steadily. At the lower exposure time (25 s), the adhesion of objects with the build-platform was found to be poor and often the object got detached while printing. After carefully observing the quality of all the printed objects, the printing condition was set as 35 s of LED exposure for the first layer followed by 23 s of exposure for each subsequent layer.

Separately, Fourier-transform infrared (FTIR) spectroscopy was carried out for the printed parts with variable UV exposure time from 11 to 25 s, along with raw liquid resin and a fully post-cured printed object to determine the curing kinetics. The FTIR spectral analysis is elucidated in ESI† the plot is presented in Fig. S4. The percentage of reaction conversion is calculated following eqn (S1) (ESI†) and is plotted in Fig. 2b. The conversion progressively increases with the extension of the UV exposure period from 11 to 25 seconds. About 75% of conversion is found for the UV exposure of 23 and 25 s. Based on the reaction conversion and flawless printed parts, we selected 23 s of UV exposure for printing of each layer of the sliced model. The post-cured printed part shows a conversion of 92%.

The glass transition (T_g) of the 3D-printed $SMP_{0.33}$, $SMP_{0.50}$, $SMP_{0.75}$ and $SMP_{1.0}$ samples were determined from the differential scanning calorimetry (DSC) study. The DSC plots of the SMPs at the temperature range of −88 to 370 °C are presented in Fig. 3a and a plot for a short temperature range (−88 to 100 °C) is shown in Fig. S5 (ESI†) indicating the T_g of the SMPs. The T_g was decreased with increasing the crosslinker concentration. The $SMP_{0.33}$, $SMP_{0.50}$, $SMP_{0.75}$ and $SMP_{1.0}$ show the T_g at ≈23, ≈18, ≈7, and ≈ −5 °C, respectively (marked in Fig. S5, ESI†). An increase in crosslinker concentration often leads to a rise in the T_g, as the mobility of the polymer becomes progressively constrained. However, in certain instances, the 'copolymerization effect' may reverse

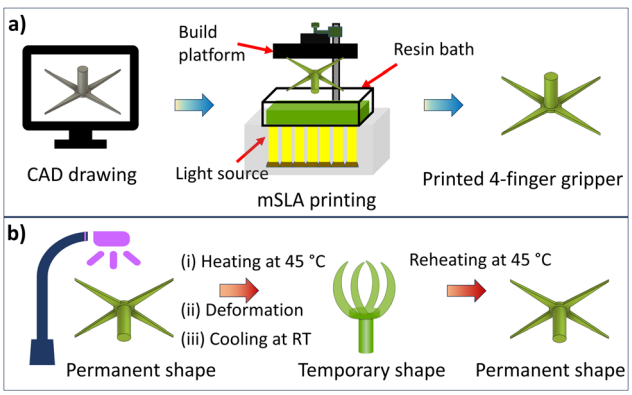

Fig. 1 Schematic presentation of (a) mSLA 3D printing and (b) one-way reversible shape transformation programming controlled by a heat lamp.

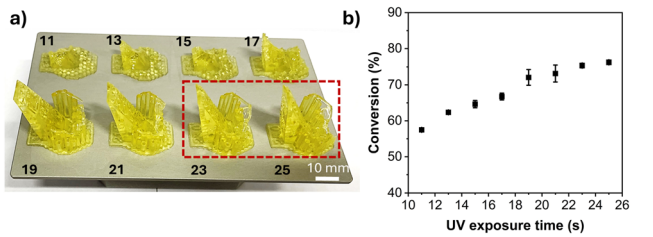

Fig. 2 (a) Printed parts with increasing LED exposure time from 11 to 25 s and (b) corresponding photopolymerization conversion studied by FTIR spectroscopy.

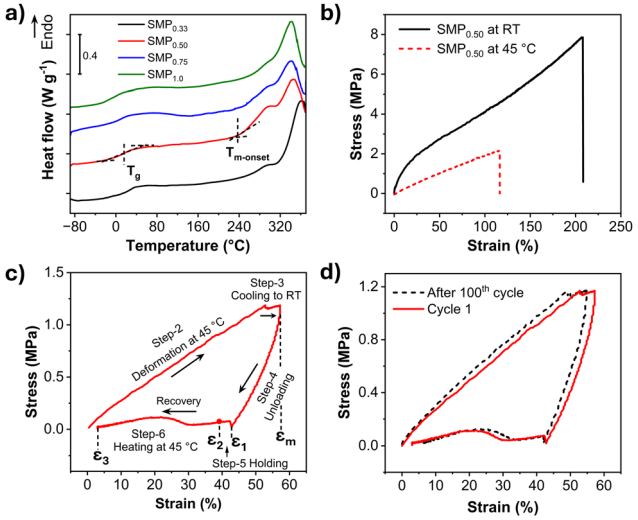

Fig. 3 (a) DSC analysis of 3D-printed $SMP_{0.33}$, $SMP_{0.50}$, $SMP_{0.75}$ and $SMP_{1.0}$. (b) Tensile testing of $SMP_{0.50}$ at RT and 45 °C, (c) stress–strain plot for a thermomechanical test cycle, and (d) cyclic thermomechanical test comparison of a specimen of $SMP_{0.50}$ after 100 cycles of shape transformation cycle.

the T_g trend depending on the type of crosslinking monomers utilized.[27] The PEGDMA, a long chain crosslink, provides a 'copolymer effect' with increasing of its concentration. It also increases the free volume of the polymer network and thus decreases the T_g as observed in our study.[28,29] The endothermic peak for melting and decomposition is prominent for all the SPMs in the temperature range 270–370 °C. The onset of melting ($T_{m\text{-onset}}$) for $SMP_{0.50}$ is marked at 240 °C. This confirms that all the SMPs are thermally stable in a wide temperature window.

After determining T_g and $T_{m\text{-onset}}$, the shape-memory effect was examined using a printed 4-finger gripper made using the different SMP resins. Based on T_g of SMPs, the grippers were programmed to a temporary shape placing it under a heat lamp bulb (300 W) for 2 min to reach a temperature ≈45 °C followed by manually bending the object to a desired shape. The deformed gripper was then cooled down to below 18 °C. The shape transformation process is shown in the schematic diagram in Fig. 1b and Video V1 (ESI†). The gripper made of $SMP_{0.50}$ (monomer to crosslinker ratio 1 : 0.50) held its temporary shape at room temperature (RT ≈19 °C) and returned to its permanent shape immediately when the temporary shape was re-heated to ≈45 °C. The gripper made of $SMP_{0.33}$ (monomer to crosslinker ratio 1 : 0.33) which was very flexible and had multiple defects in its structure, did not recover its permanent shape upon reheating. It shows an irreversible shape transformation. The gripper made of $SMP_{0.75}$ (monomer to crosslinker ratio 1 : 0.75) showed shape-memory behaviour similar to $SMP_{0.50}$, however, it was found to be unable to hold the temporary shape for a prolonged period. The gripper made of $SPM_{1.0}$ (monomer and crosslinker ratio 1 : 1) showed no shape-memory behaviour as it was unable to hold any temporary shape. The fast recovery of $SMP_{0.75}$ and $SMP_{1.0}$ is related to the crosslinking density and T_g of the polymers. The higher amount of crosslinker (PEGDMA) in the $SMP_{0.75}$ and $SMP_{1.0}$ resins increased the crosslinking density of the polymers. This high crosslinking density resulted in fast creep recovery without holding the temporary shape.[30] This study elucidates that $SMP_{0.5}$ was the only formulation found to exhibit typical shape-memory behaviour in the temperature window of 15–45 °C. The shape transformation operation of the gripper $SMP_{0.50}$ was examined for 100 cycles and no defect was noticed in its parts.

The cyclic thermomechanical test was performed to confirm the shape-memory behaviour of $SMP_{0.50}$. Before setting thermomechanical tensile test cycles, tensile testing was carried out employing the printed dog bone tensile specimens (ASTM D638 type-IV)[31] from $SMP_{0.50}$ (Fig. S6, ESI†) to determine the tensile strength, Young's modulus and elongation-at-break at RT and 45 °C in a universal testing machine (UTM). These data served to determine the experimental parameters for cyclic thermomechanical testing. The stress–strain plots from the tensile test are shown in Fig. 3b. The Young's modulus, tensile strength and elongation-at-break were calculated to be 16.11 ± 0.35 MPa, 8.86 ± 1.47 MPa and 220.83 ± 19.42% at RT, and 2.47 ± 0.03 MPa, 2.32 ± 0.25 MPa, and 117.64 ± 2.34% at 45 °C, respectively. The cyclic thermomechanical test was programmed following a modified procedure reported by Wu *et al.*[32] consisted of seven steps as stated in Table S1 (ESI†). In short, the steps are (1) heating the specimen at 45 °C for 2 min, (2) elongation up to a stress limit of 1.18 MPa (load 30 N), (3) cooling to RT holding the load of 30 N, (4) releasing the load to 0.5 N, (5) holding isothermally at RT for 2 min (6) reheating to 45 °C and holding for 2 min at ≈45 °C and (7) cooling of the specimen to RT. The resulting stress–strain plot for step (2)–(6) is shown in Fig. 3c. The specimen achieved a maximum strain, ε_m after step-3 once it was cooled to RT. During unloading at step-4, the specimen recovered a certain strain and the residual stain remains ε_1. At the holding step-5, the specimen further recovered strain due to creep recovery and possessed a residual strain ε_2. The specimen reached a final residual strain, ε_3 known as the recovered strain which was retrieved through the reheating at step-6. It is to be noted that during the cyclic thermomechanical test, the specimen was cooled to RT (≈ 19 °C) however, to arrest the temporary shape for prolonged time, it is important to cool the specimen below T_g (18 °C) at step-3. This results in a fast creep recovery of (ε_1–ε_2). The instant shape fixity ratio (R_f) and the shape recovery ratio (R_r) are determined from eqn (S2) and (S3) (ESI†), respectively from the obtained ε_m, ε_1, ε_2, and ε_3.[32] The instant shape fixity ratio and shape recovery of $SMP_{0.50}$ are calculated to be 78 ± 3 and 91 ± 2%, respectively. A comparison of cyclic thermomechanical plots of $SMP_{0.75}$ and $SMP_{0.50}$ is shown in Fig. S7a (ESI†) with an explanation included. This cyclic testing was performed for 10 cycles as shown in Fig. S7b (ESI†). The stress–strain plots followed a similar path as of cycle-1 with trivial deviation. The specimen is found to undergo near-identical shape transformation cycles. To determine a quantitative cyclic stability, the specimen was taken out from the tensile testing equipment, and the shape transformation cycle was applied continuously for 100 cycles. The tensile specimen was bent into a 'U' shape for each cycle and recovered its original shape as shown Fig. S8 (ESI†). The specimen was examined again with the tensile testing equipment and the cyclic thermomechanical stress–strain plot was compared with cycle 1 (Fig. 3d). The specimen shows shape fixity ratio of 77% and shape recovery of 84% even after such

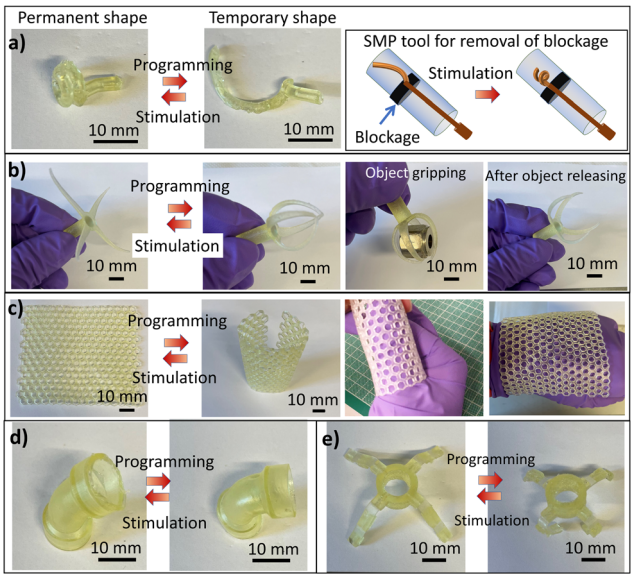

Fig. 4 Photographs of different 3D-printed SMP tools and their shape transformation, and applications. (a) A rod with a spiral end, (b) 4-finger gripper, (c) a flexible sheet with honeycomb patterns, (d) pipe elbow and (e) 4-legged object.

a high-angle shape transformation for 100 cycles. This suggests that $SMP_{0.50}$ can be used for multiple shape-memory cycles in robotic applications. The shape-changing mechanism is explained by a schematic in Fig. S9 (ESI†).

Several 3D-printed tools using $SMP_{0.50}$ were programmed to demonstrate simple soft robotic applications such as a rod with spiral end for removal of blockage from a pipe (Fig. 4a), 4-finger gripper to hold and release objects (Fig. 4b), a flexible sheet with honeycomb patterns for customized orthopaedic cast on fingers/wrist instead of hard pasters (Fig. 4c), a pipe elbow to join two pipes at any angle (Fig. 4d) and a 4-legged object for walking (Fig. 4e). The programming steps involved photothermal heating for 2 min, followed by deformation to the desired shape and cooling back to RT to arrest the shape. The printed tools could undergo infinite conformation changes that facilitate application in situations as necessitated. 3D printing in particular enables the design and printing of any customized shape with the formulated resin. The light-responsive transformation is shown to facilitate their application in real-life practical situations.

In this work, we demonstrated mSLA printing of a customized resin formulated from acrylate and methacrylate derivatives to obtain photothermal active SMP for soft robotics applications. The SMP shows reversible shape transition with defined programming within a temperature range of 15–45 °C. By carefully varying the monomer to crosslinker ratio, it is found that a mass ratio of 1 : 0.5 of BMA and PEGDMA creates a polymer with the desired shape memory behaviour. 3D-printed SMP tools were demonstrated to be applicable for several shape transformation-based operations. In future, to facilitate the application of soft robots in industrial and medical operations, electrically controlled heating and cooling can be integrated to remotely control the robotic actuation.

S. K.-N: conceptualization, funding acquisition, resources, supervision, writing – review & editing and K. G.: conceptualization, data curation, formal analysis, funding acquisition, investigation, methodology, project administration, validation, visualization, writing – original draft.

S. K.-N. acknowledges funding from UK Research and Innovation (UKRI) under the UK government's Horizon Europe funding guarantee (EP/Y032535/1). K. G. acknowledges funding from the Royal Society Newton International Fellowship (NIF\R1\221866).

Data availability

Supporting data for this paper is available at the University of Cambridge Apollo data repository (DOI: 10.17863/CAM.112845).

Conflicts of interest

There are no conflicts to declare.

Notes and references

1 P. Dario, E. Guglielmelli and C. Laschi, *J. Robot. Syst.*, 2001, **18**, 673–690.
2 J. M. Jordan, *Robots*, MIT Press, 2016.
3 D. Silvera-Tawil, *SN Comput. Sci.*, 2024, **5**, 189.
4 S. B. Niku, *Introduction to robotics: analysis, control, applications*, John Wiley & Sons, 2020.
5 C. Laschi, B. Mazzolai and M. Cianchetti, *Sci. Robot*, 2016, **1**, eaah3690.
6 G. M. Whitesides, *Angew. Chem., Int. Ed.*, 2018, **57**, 4258–4273.
7 J. Zhang, Q. Jing, T. Wade, Z. Xu, L. Ives, D. Zhang, J. J. Baumberg and S. Kar-Narayan, *ACS Appl. Mater. Interfaces*, 2024, **16**, 6485–6494.
8 M. Zastrow, *Nature*, 2020, **578**, 20–23.
9 Q. Ge, H. J. Qi and M. L. Dunn, *Appl. Phys. Lett.*, 2013, **103**, 131901.
10 A. Tariq, Z. U. Arif, M. Y. Khalid, M. Hossain, P. I. Rasool, R. Umer and S. Ramakrishna, *Adv. Eng. Mater.*, 2023, **25**, 2301074.
11 Z. U. Arif, M. Y. Khalid, A. Tariq, M. Hossain and R. Umer, *Giant*, 2023, 100209.
12 P. Kumar, P. Suryavanshi, S. K. Dwivedy and S. Banerjee, *J. Mol. Liq.*, 2024, 125553.
13 X. Wang, M. Jiang, Z. Zhou, J. Gou and D. Hui, *Composites, Part B*, 2017, **110**, 442–458.
14 C. W. Hull, *Res. Technol. Manage.*, 2015, **58**, 25–30.
15 P. J. Bártolo, *Stereolithography: materials, processes and applications*, Springer Science & Business Media, 2011.
16 W. Zhao, Z. Wang, J. Zhang, X. Wang, Y. Xu, N. Ding and Z. Peng, *Adv. Mater. Technol.*, 2021, **6**, 2001218.
17 Q. Ge, A. H. Sakhaei, H. Lee, C. K. Dunn, N. X. Fang and M. L. Dunn, *Sci. Rep.*, 2016, **6**, 31110.
18 B. Zhang, W. Zhang, Z. Zhang, Y.-F. Zhang, H. Hingorani, Z. Liu, J. Liu and Q. Ge, *ACS Appl. Mater. Interfaces*, 2019, **11**, 10328–10336.
19 C. Sun, N. Fang, D. M. Wu and X. Zhang, *Sens. Actuators, A*, 2005, **121**, 113–120.
20 Y. Pan, X. Zhao, C. Zhou and Y. Chen, *J. Manuf. Process.*, 2012, **14**, 460–470.
21 J. L. Kricke, *et al.*, *Virtual Phys. Prototyping*, 2023, **18**, e2251017.
22 E. Sachyani Keneth, A. Kamyshny, M. Totaro, L. Beccai and S. Magdassi, *Adv. Mater.*, 2021, **33**, 2003387.
23 A. Nishiguchi, H. Zhang, S. Schweizerhof, M. F. Schulte, A. Mourran and M. Möller, *ACS Appl. Mater. Interfaces*, 2020, **12**, 12176–12185.
24 E. Sachyani Keneth, R. Lieberman, M. Rednor, G. Scalet, F. Auricchio and S. Magdassi, *Polymers*, 2020, **12**, 710.
25 Y. Chen, X. Zhao, Y. Li, Z.-Y. Jin, Y. Yang, M.-B. Yang and B. Yin, *J. Mater. Chem. C*, 2021, **9**, 5515–5527.
26 https://help.prusa3d.com/article/resin-calibration-sl1-sl1s_112182.
27 S. Loshaek, *J. Polym. Sci.*, 1955, **15**, 391–404.
28 J. Bicerano, R. L. Sammler, C. J. Carriere and J. T. Seitz, *J. Polym. Sci., Part B: Polym. Phys.*, 1996, **34**, 2247–2259.
29 A. R. Kannurpatti, J. W. Anseth and C. N. Bowman, *Polymer*, 1998, **39**, 2507–2513.
30 K. V. Rao, G. S. Ananthapadmanabha and G. N. Dayananda, *J. Mater. Eng. Perform.*, 2016, **25**, 5314–5322.
31 ASTM International, ASTM standard, D638-22. https://www.astm.org/d0638-22.html.
32 X. L. Wu, W. M. Huang and H. X. Tan, *J. Polym. Res.*, 2013, **20**, 1–11.